宮崎大輔, 池内克史,
"偏光解析による透明物体の形状計測,"
情報処理学会コンピュータビジョンとイメージメディア研究会,
東京, 2005.05 to appear

偏光解析による透明物体の形状計測

宮崎 大輔　池内 克史

東京大学 情報理工学系研究科 コンピュータ科学専攻

あらまし　コンピュータグラフィクスやバーチャルリアリティの技術が様々な場面で応用されるにしたがって，現実物体の３次元形状を計測する手法の重要性が高まってきた．しかしながら，ガラスやアクリルといった透明な物体の３次元形状を計測する手法はわずかしか提案されておらず，一般に普及されるには至っていない．本論文では，偏光解析をもとに透明物体の表面形状を計測する三つの手法を提案する．一つ目の手法では，熱力学の知識ももちいて透明物体の表面形状を決定する．二つ目の手法では，微分幾何学の知識ももちいて透明物体の表面形状を決定する．三つ目の手法では，透明物体の表面形状の初期値をもとに，反復計算により真の表面形状を決定する．

Shape Estimation of Transparent Objects by using Polarization Analyses

Daisuke Miyazaki and Katsushi Ikeuchi

Computer Science, Graduate School of
Information Science and Technology, The University of Tokyo

Abstract　Today, techniques developed in the field of computer graphics and virtual reality are applied in many scenes, resulting the method of measuring 3D shape of real objects to be more and more important. However, less methods are proposed to measure 3D shape of transparent objects such as glasses and acrylics. In this paper, I propose three kinds of method, which estimate the surface shape of transparent object by using polarization analysis. The first method determines the surface shape of transparent object by also using the knowledge established in the research field of thermodynamics. The second method determines the surface shape of transparent object by also using the knowledge established in the research field of differential geometry. The third method determines the true surface shape of transparent object by an iterative computation by giving an initial value of the surface shape.

1. Introduction

In the field of computer vision, few methods have been proposed for estimating the shape of transparent objects, because of the difficulty of treating with the internal interreflection(=internal reflection or interreflection), which are the phenomena that the light not only reflects at the surface of the transparent object but also transmits into the object and causes multiple reflection and transmission inside it. This paper presents three methods for estimating the surface shape of transparent objects by analyzing the polarization of transparent objects.

1.1. Related Work

Polarization is a phenomenon in which the light oscillates in one direction. Recently, research to estimate the object shape by using polarization has increased. Kosikawa and Shirai [1] proposed to use the degree of polarization, employing circulary polarized light sources to determine the surface normal of specular polyhedrons. They used a method called Mueller calculus to calculate the polarization state of the light. Wolff and Boult [2] indicated that the surface normal of the object surface is constrained by analyzing the polarization of the object, and estimated the surface normal of a planer glass from

two views. Rahmann [3] estimated the orientation of a flat object and the position of the light source by polarization analysis of single view. Rahmann also [4] addressed the potential of recovering the shape of specular surfaces from polarization. Later, Rahmann and Canterakis [5] estimated the shape of specular objects from two or more views. Also, they proved that the quadratic shape of specular objects can be estimated from two views [6]. Drbohlav and Šára [7] estimated the shape of diffuse objects by combining the polarization analysis and the photometric stereo. Miyazaki et al. [8] estimated the shape and reflectance of specular objects and the illuminant direction from one view. Saito et al. [9] employed the analysis of the degree of polarization and developed a method with which the surface of a transparent object could be determined; however, the degree of polarization provided two candidates of surface normal, and they did not solve this ambiguity. Unfortunately, because these methods do not consider internal interreflections, they do not provide sufficient accuracy for estimating the shape of transparent objects.

A little methods which estimate the 3D shape of transparent objects have been proposed. Murase [10] estimated the shape of water surface by analyzing the undulation of the water surface. Hata et al. [11] estimated the surface shape of transparent objects by analyzing the deformation of the light projected onto the transparent objects. Ohara et al. [12] estimated the depth of the edge of transparent object by using shape-from-focus. Ben-Ezra and Nayar [13] estimated the parameterized surface shape of transparent objects by using structure-from-motion. These methods, however, do not estimate arbitrary shapes of transparent objects.

1.2. Overview

Saito et al. [9] employed the analysis of the degree of polarization and developed a method with which to measure the surface of a transparent object. Then, by measuring the DOP(=degree of polarization) of a transparent object, they determined surface normals. Unfortunately, however, the DOP provides two solutions corresponding to one DOP.

In this paper, I propose to disambiguate these two solutions by two methods. One is to introduce the DOP of the thermal radiation, and the other is to introduce the polarization analysis by considering the differential-geometrical property of the object surface. Saito's method and these two methods do not consider the effect of internal interreflection, hence, I propose another method to estimate the surface shape of transparent objects more precisely by considering both reflection and transmission.

The paper is organized as follows. In Section 2, I present the background theory of polarization and then develop an underlying algorithm to determine surface normal up to two possible incident angles, using the polarization. I describe the first method in Section 3: This method, using thermal radiation, solves the ambiguity problem of Saito's method and obtain an unique surface normal of transparent object. I describe the second method in Section 4: This method, using differential geometry, solves the ambiguity problem of Saito's method and obtain an unique surface normal of transparent object which is also done in the first method. I describe the third method in Section 5: This method, using polarization raytracing, solves the internal interreflection problem of Saito's method, the first method, and the second method. In Section 6, I describe the apparatus of these three methods and the experimental results of them. Section 7 concludes the paper.

2. Polarization Analysis

2.1. Fresnel Reflection

In this section, I present a brief overview of the basic equation of reflection and refraction [14]. In Figure 1, let us consider the case in which a light hits the interface surface between two materials, the refractive indices of which are denoted as n_1 and n_2, respectively. One part of the light is reflected from the interface surface, while another part penetrates the surface and is refracted when it enters the second material. The plane including the surface normal and the incident light ray is called the POI(=plane of incidence). I identify the parallel and perpendicular components to the POI as $\parallel$ and $\perp$, respectively. The incident, reflecting, and transmitting angles are defined as θ_1, θ_1', and θ_2, respectively, as shown in Figure 1. Since I focus on optically smooth transparent objects, the incident angle and the reflecting angle will be

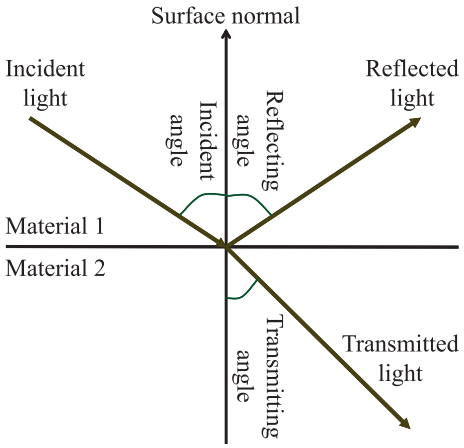

Fig. 1: Reflection, refraction, and transmission.

the same $\theta_1 = \theta_1'$. θ_1 and θ_2 is related by Snell's law,

$$n_1 \sin\theta_1 = n_2 \sin\theta_2 \,. \tag{1}$$

I define the parallel and perpendicular intensity reflectivities, $R_{||}$ and $R_\perp$, respectively, as

$$R_{||} = \frac{\tan^2(\theta_1 - \theta_2)}{\tan^2(\theta_1 + \theta_2)}$$
$$R_\perp = \frac{\sin^2(\theta_1 - \theta_2)}{\sin^2(\theta_1 + \theta_2)} \quad . \tag{2}$$

From the above equation, an incident angle to make $R_{||} = 0$ can be obtained. This incident angle is referred to as the Brewster angle, θ_B. The Brewster angle is obtained by substituting $\theta_1 + \theta_2 = \pi/2$ (namely, $R_{||} = 0$) into Snell's equation as

$$\tan\theta_B = \frac{n_2}{n_1} \,. \tag{3}$$

Once the reflecting angle and the POI angle are known, I can determine the surface normal with respect to the viewer, as shown in Figure 2. I will denote the POI angle and the reflecting angle as ψ and θ, respectively, and determine these two angles by using the degree of polarization of reflected light.

2.1.1. POI Angle

As shown in Equation (2), the intensity of the reflected light varies depending on the direction of oscillation in the plane of oscillation; therefore, a difference can be observed when the polarization filter is rotated in front of a CCD camera. The variance is described as a sinusoidal function of rotation angles. I will denote the maximum and minimum brightness in the observed intensities as

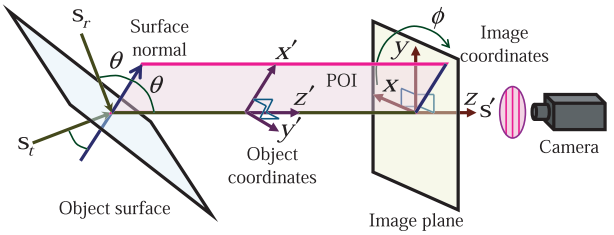

Fig. 2: Reflected and transmitted light observed by the camera.

$I_{\max}$ and $I_{\min}$. Given that the sum of the maximum and minimum brightness is the total brightness of the reflected light I_{spec},

$$I_{\max} = \frac{R_\perp}{R_{||} + R_\perp} I_{\text{spec}}, \quad I_{\min} = \frac{R_{||}}{R_{||} + R_\perp} I_{\text{spec}} \,. \tag{4}$$

By this equation, the direction parallel to the plane of incidence provides the minimum brightness $I_{\min}$. Namely, by measuring the angle where the minimum brightness is observed, I can determine the POI angle ψ ($0 \le \psi < 2\pi$). POI angle is determined as the angle between $+x$-axis and POI, from $+x$-axis to $+y$-axis, as shown in Figure 2. There are two possible POI angles, ψ_{LO} and ψ_{HI}, which are definable as $\psi_{\text{HI}} = \psi_{\text{LO}} + \pi$, where $0 \le \psi_{\text{LO}} < \pi$ and $\pi \le \psi_{\text{HI}} < 2\pi$. Surface normal can be represented in polar coordinates with zenith angle θ and azimuth angle ϕ. Azimuth angle ϕ equals to ψ_{LO} or ψ_{HI}.

Since I assume that the object is a closed, smooth object, I can determine the surface normal at the occluding boundary; the surface normal heads for the outside of the shape of the projection of the object at the occluding boundary. By using the ϕ at the occluding boundary as an initial condition, I propagate the constraint of ϕ throughout the surface and, finally, determine the value of ϕ, whether it is $\phi = \psi_{\text{LO}}$ or $\phi = \psi_{\text{HI}}$, over the entire surface, assuming that all local parts of the surface are not concave toward the camera direction.

2.1.2. Incident Angle

The definition of the degree of polarization is,

$$\rho = \frac{I_{\max} - I_{\min}}{I_{\max} + I_{\min}} \,. \tag{5}$$

The degree of polarization is 0 when the light is unpolarized, whereas it is 1 when the light is linearly polarized.

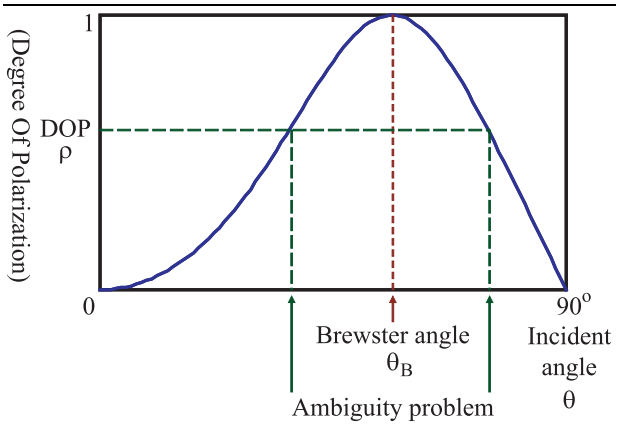

Fig. 3: Relation between the degree of polarization and the incident angle ($n = 1.5$).

The linearly polarized light is observed when the incident angle and the reflecting angle are at the Brewster angle.

By substituting Equation (4) and (2) into Equation (5) with Snell's law, I can represent the degree of polarization ρ as

$$\rho = \frac{2\sin^2\theta\sqrt{n^2 - \sin^2\theta - n^2\sin^2\theta + \sin^4\theta}}{n^2 - \sin^2\theta - n^2\sin^2\theta + 2\sin^4\theta}. \quad (6)$$

The degree of polarization is a function of the refractive index n ($= n_2/n_1$) and the incident angle θ ($= \theta_1$) ($0 \leq \theta \leq \pi/2$). Threfore, by obtaining the degree of polarization from the data, I can determine the incident angle θ, given the refractive index n.

Figure 3 shows the relationship between the degree of polarization and the incident angle. Here, the horizontal and vertical axes denote the incident angle and the degree of polarization, respectively. I can obtain the incident angle from the observed degree of polarization even if I do not know the intensity of the light source. The function has an extremum at the Brewster angle. From this function, an observed degree of polarization provides two possible incident angles, except at the Brewster angle. It is necessary to have a method to resolve this ambiguity. In this paper, I propose to solve this problem by two methods, one by considering the polarization of far infrared light (Section 3), and the other by comparing two polarization data through rotating the object (Section 4).

2.2. Polarization Raytracing

2.2.1. Mueller Calculus

A conventional raytracing method renders a 2D image from 3D geometrical shape data of transparent objects or other kind of objects. In this paper, I call the raytracing method which considers the polarization effect the polarization raytracing method. The algorithm of the polarization raytracing method can be divided into two parts. For the first part, the calculation of the propagation of the ray, I employ the same algorithm used in the conventional raytracing method. For the second part, the calculation of the polarization state of the light, the direct implementation of Section 2.1 is possible, however, there are more effective methods to calculate the polarization: Mueller calculus [15], Jones calculus [15], and the method which uses the coherence matrix [14]. In this paper, I employ Mueller calculus, because of its simplicity of description, along with its ease of understanding and implementation. These three methods have almost identical functions; thus, all discussions presented in this paper are also applicable to other calculi. I will present a brief overview of Mueller calculus in the following pages; however, I will leave the details to the literature [15].

In Mueller calculus, the polarization state of the light is represented as Stokes vector $\mathbf{s} = (s_0, s_1, s_2, s_3)^T$. The Stokes vector is a 4D vector. Its first component s_0 represents the intensity of the light; its second component s_1 represents the horizontal power of the linear polarization; its third component s_2 represents the $+45°$-oblique power of the linear polarization; and its fourth component s_3 represents the power of the right circular polarization. The Mueller matrix $\mathbf{M}$, which is 4×4 matrix, represents how the object changes the polarization state of the light. The operation of Mueller calculus is a linear operation.

2.2.2. Mueller Matrix

First, I introduce a method for calculating the polarization state of the reflected light and the transmitted light when the POI angle is $0°$; after that, I introduce a method for the case when the POI angle is not $0°$.

Mueller Matrices of reflection $\mathbf{R}$ and transmission $\mathbf{T}$ when the POI angle is $0°$ are represented as follows:

$$\mathbf{R} = \begin{pmatrix} (R_{\|} + R_{\perp})/2 & (R_{\|} - R_{\perp})/2 & 0 & 0 \\ (R_{\|} - R_{\perp})/2 & (R_{\|} + R_{\perp})/2 & 0 & 0 \\ 0 & 0 & \sqrt{R_{\|}R_{\perp}} & 0 \\ 0 & 0 & 0 & \sqrt{R_{\|}R_{\perp}} \end{pmatrix}$$

$$\mathbf{T} = \begin{pmatrix} (T_{||} + T_{\perp})/2 & (T_{||} - T_{\perp})/2 & 0 & 0 \\ (T_{||} - T_{\perp})/2 & (T_{||} + T_{\perp})/2 & 0 & 0 \\ 0 & 0 & \sqrt{T_{||}T_{\perp}} & 0 \\ 0 & 0 & 0 & \sqrt{T_{||}T_{\perp}} \end{pmatrix} . \quad (7)$$

Therefore, if I have a light ray with the Stokes vector $\mathbf{s}$ impinged on an object, then the Stokes vector of reflected light will be $\mathbf{R}\mathbf{s}$, when the POI angle is $0°$. The same thing can also be said of the transmitted light.

Figure 2 illustrates the case when the POI angle is ψ. Figure 4 explains how to calculate the reflected light for this case. The reflection matrix $\mathbf{R}$ is always multiplied to the Stokes vector whose POI angle is transformed to $0°$. So, I first rotate the incident Stokes vector $\mathbf{s}$ with the angle $-\psi$. After that, $\mathbf{R}$ is multiplied to the transformed Stokes vector. Finally, the Stokes vector is rotated again with the angle ψ in order to restore the original coordinates. The resulting Stokes vector $\mathbf{s}'$ is as follows:

$$\mathbf{s}' = \mathbf{C}(\psi)\mathbf{R}\mathbf{C}(-\psi)\mathbf{s} \quad , \quad (8)$$

where rotation matrix $\mathbf{C}$ is given as:

$$\mathbf{C}(\psi) = \begin{pmatrix} 1 & 0 & 0 & 0 \\ 0 & \cos 2\psi & -\sin 2\psi & 0 \\ 0 & \sin 2\psi & \cos 2\psi & 0 \\ 0 & 0 & 0 & 1 \end{pmatrix} . \quad (9)$$

As for the case in Figure 2, observed light is a composition of reflected light and transmitted light. Therefore, the Stokes vector $\mathbf{s}'$ of the observed light is calculated as follows:

$$\mathbf{s}' = \mathbf{C}(\psi)\mathbf{R}\mathbf{C}(-\psi)\mathbf{s}_r + \mathbf{C}(\psi)\mathbf{T}\mathbf{C}(-\psi)\mathbf{s}_t \quad , \quad (10)$$

where Stokes vectors of the incident light are represented as $\mathbf{s}_r$ and $\mathbf{s}_t$, and where $\mathbf{s}_r$ and $\mathbf{s}_t$ represent the lights which are set in the origin of the reflection and transmission, respectively.

2.2.3. Phase Shift

If an incident angle is larger than the critical angle, then the light does not transmit and totally reflects. This phenomenon is called total reflection and occurs when the light is inside the object. Critical angle is defined in following equation:

$$\sin\theta_C = \frac{n_2}{n_1} . \quad (11)$$

Here, n_1 and n_2 are the refractive indices of two materials, where $n_1 > n_2$; for example, n_1 and n_2 might be the refractive indices of the object and the air, respectively. Phase of the reflected light shifts when the total reflection occurs. Therefore, for the total reflection, the following matrix $\mathbf{D}$ is used instead of the reflection Mueller matrix $\mathbf{R}$:

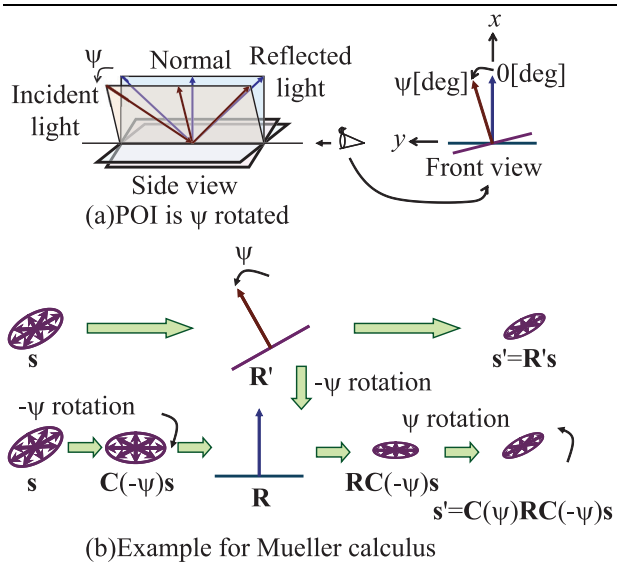

Fig. 4: Calculation example of rotation Mueller matrix for reflection.

$$\mathbf{D}(\delta) = \begin{pmatrix} 1 & 0 & 0 & 0 \\ 0 & 1 & 0 & 0 \\ 0 & 0 & \cos\delta & \sin\delta \\ 0 & 0 & -\sin\delta & \cos\delta \end{pmatrix} , \quad (12)$$

where δ is the amount of the phase shift, calculated by using the following formula:

$$\tan\frac{\delta}{2} = \frac{\cos\theta\sqrt{\sin^2\theta - n^2}}{\sin^2\theta} , \quad (13)$$

where θ is the incident angle and $n = n_2/n_1$, where n_1 and n_2 are the refractive indices of the object and the air, respectively.

When the incident angle is less than the Brewster angle, the phase of the reflected light will be inverted; thus, the matrix $\mathbf{D}(180°)$ should be multiplied from the left to the reflection Mueller matrix.

2.2.4. Degree of Polarization

Because the linear polarizer is used in this research, the fourth parameter s_3 of the Stokes vector cannot be determined. The relationship between the Stokes vector

$(s_0, s_1, s_2)^T$ and $I_{\max}$, $I_{\min}$, ψ is:

$$\begin{pmatrix} s_0 \\ s_1 \\ s_2 \end{pmatrix} = \begin{pmatrix} 1 & 0 & 0 \\ 0 & \cos 2\psi & -\sin 2\psi \\ 0 & \sin 2\psi & \cos 2\psi \end{pmatrix} \begin{pmatrix} I_{\min} + I_{\max} \\ I_{\min} - I_{\max} \\ 0 \end{pmatrix}, \quad (14)$$

where $I_{\max}$ and $I_{\min}$ are defined in Section 2.1, and ψ is a POI angle also defined in Section 2.1. The degree of polarization represents how much the light is polarized and is defined as follows:

$$\hat{\rho} = \frac{\sqrt{s_1^2 + s_2^2 + s_3^2}}{s_0} \quad . \quad (15)$$

However, linear polarizer can only calculate the following degenerated DOP:

$$\rho = \frac{I_{\max} - I_{\min}}{I_{\max} + I_{\min}} = \frac{\sqrt{s_1^2 + s_2^2}}{s_0} \quad . \quad (16)$$

For the remainder of this paper, I refer to the ratio calculated by Equation (16) as DOP.

2.2.5. Illumination Distribution

In this paper, I assume that all light sources are unpolarized. In Section 5, I assume that the intensity of the illumination is known.

3. Shape Estimation of Transparent Objects by using Polarization Analysis and Thermal Radiation

In this section, I explain the method to solve the ambiguity by introducing thermal radiation.

3.1. Introduction

Section 2 explained how to calculate surface normal from polarization data. However, there exist an ambiguity problem of determining the zenith angle θ from the DOP ρ, since the correspondence between ρ and θ is not one-to-one but one-to-two. Fortunately, the correspondence between the DOP and the zenith angle will be one-to-one if we obtain the DOP of the thermal radiation observed in the infrared light domain. In this section, I explain how to obtain the correct surface normal by disambiguating θ by analyzing the thermal radiation by using the knowledge in thermodynamics and optics.

3.2. Thermal Radiation

Any object who has a positive temperature will radiate energy. Let us explain the polarization phenomenon of thermal radiation by considering the light emitted from inside the object [16–21]. Thermal radiation emitted from inside the object is transmitted through the interface surface and radiated into the air.

For the explanation in this section, suppose material 1 be the object and material 2 be the air, as shown in Figure 1. In this case, $\theta_2 > \theta_1$. The refractive index of the object relative to the air will be $n = n_1/n_2$. θ_2 is the emitting angle.

I can define the parallel and perpendicular intensity ratios of transmission, $T_{||}$ and $T_{\perp}$, as

$$T_{||} = \frac{\sin 2\theta_1 \sin 2\theta_2}{\sin^2(\theta_1 + \theta_2)\cos^2(\theta_1 - \theta_2)}$$
$$T_{\perp} = \frac{\sin 2\theta_1 \sin 2\theta_2}{\sin^2(\theta_1 + \theta_2)} \quad (17)$$

Therefore, $I_{\max}$ and $I_{\min}$ will be written by using the total energy of the emitted light, W, as

$$I_{\max} = \frac{T_{||}}{T_{||} + T_{\perp}} W, \qquad I_{\min} = \frac{T_{\perp}}{T_{||} + T_{\perp}} W \, . \quad (18)$$

The degree of polarization of thermal radiation ρ_{IR} will be as follows:

$$\rho_{\mathrm{IR}} = \frac{I_{\max} - I_{\min}}{I_{\max} + I_{\min}} = \frac{T_{||} - T_{\perp}}{T_{||} + T_{\perp}} \quad . \quad (19)$$

3.3. Degree of Polarization of Thermal Radiation

Figure 5(a) shows the relation between the DOP, ρ_{IR}, and the emitting angle, θ. As shown in this figure, there is a 1-to-1 correspondence between the DOP and the emitting angle. Therefore, once I measure the DOP in an infrared light, I can uniquely determine the emitting angle. For the sake of comparison, Figure 5(b) represents the visible light condition. In this function, as mentioned, one DOP value corresponds to two emitting angles.

Unfortunately, however, the DOP in emitted infrared light is much smaller than that in reflected visible light. Thus, I propose to use both visible and infrared light. By using visible light, I can achieve a highly accurate measurement with ambiguity. By using the infrared light, I discriminate between the two sides.

4. Shape Estimation of Transparent Objects by using Polarization Analysis and Differential Geometry

In this section, I introduce the method of solving the ambiguity by rotating the object.

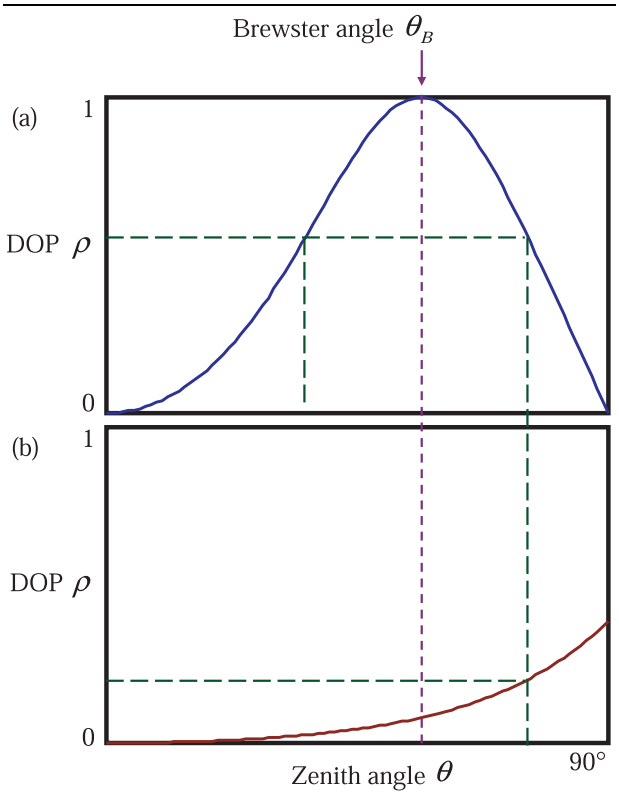

Fig. 5: DOP of (a)thermal radiation (infrared light) ($n = 1.5$), and (b)reflected light (visible light) ($n = 1.5$)

4.1. Introduction

Section 2 explained how to calculate surface normal from polarization data. In that section, I indicated that there exists an ambiguity problem: the surface normal cannot be uniquely determined from several possible surface normals obtained by the measurement. As I discussed in Section 2.1.2, the zenith angle θ of the surface normal can be determined from the degree of polarization ρ, though there is an ambiguity problem. In this section, I explain how to disambiguate the ambiguity of θ and to obtain the correct surface normal by rotating the object and analyzing the differential-geometrical property of the surface, observing the object in visible light domain, which is a different approach from the method in Section 3 but same purpose. If the reader of this paper is not familiar to the fundamental theory of Gaussian geometry, please read the literature [22, 23].

4.2. Brewster Segmentation

I have explained how to obtain the DOP of the light reflected on the object surface in Section 2. Now, I segment the data of DOP into some regions bounded by the Brewster angle θ_B. Points of the Brewster angle have no ambiguity and the DOP ρ is equal to 1.

Since I assume that the object is a closed, smooth object, the curve connected by points of the Brewster angle will form a closed curve. This curve is sometimes thick, sometimes thin, and sometimes a combination of both. I denote a point where the zenith angle is equal to Brewster angle as the "Brewster point" and the closed curve consisting of Brewster points as the "Brewster curve." I define the segmentation by Brewster curves as "Brewster segmentation."

The incident angle of all points in the region segmented through the Brewster segmentation, is either greater than the Brewster angle or smaller than the Brewster angle. Therefore, I can uniquely determine all the incident angles in the region if I can disambiguate only one point in the region.

Now, let us consider the surface regions segmented with regard to the Brewster angle with a Gaussian sphere representation. The regions generated by Brewster segmentation can be grouped into three classes(Figure 6):

1. B-E region — a region enclosed within a Brewster curve and an occluding boundary (mapped to the Equator on the Gaussian sphere),
2. B-N region — a region enclosed only with a Brewster curve and containing a surface normal toward the viewer direction (mapped to the North Pole on the Gaussian sphere),
3. B-B region — a region enclosed only with one or more Brewster curve(s) and neither containing occluding boundary nor the surface normal facing the viewer.

The result of the Brewster segmentation of the object depicted in Figure 7 is shown in Figure 8. Figure 8(a) is a gray image of the DOP, where $\rho = 0$ is represented as black and $\rho = 1$ is represented as white. Figure 8(b) is the result of the Brewster segmentation of Figure 8(a). There are two Brewster curves and one occluding boundary and one each of B-E region, B-B region, and B-N region.

4.2.1. B-E Region

The B-E region is the region which includes the occluding boundary whose zenith angle θ equals $90°$. On the

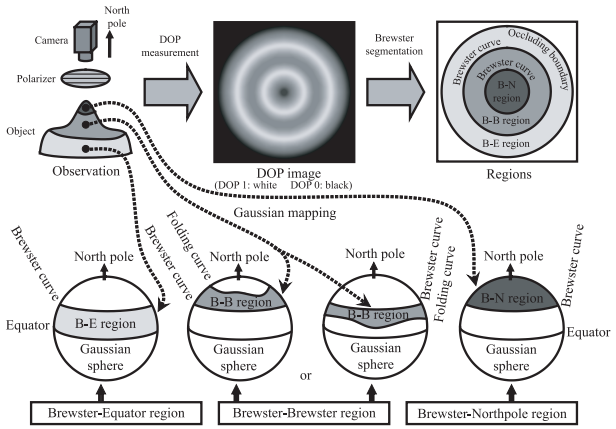

Fig. 6: Gaussian mapping and regions.

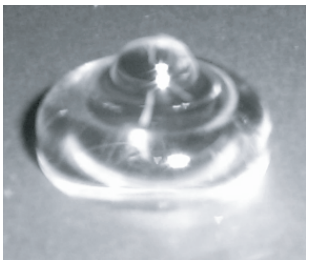

Fig. 7: A photograph of the bell-shaped object.

Gaussian sphere, B-E region is enclosed within a small circle mapped from the Brewster curve and an equator mapped from the occluding boundary. The zenith angle of all the points of B-E region is located between the Brewster angle and the occluding angle, $90°$. The graph described in Figure 3 indicates that the correspondence between θ and ρ is one to one at this region, $\theta_B \leq \theta \leq 90°$; thus, I can uniquely determine the incident angle from an observed DOP, ρ.

I assume that the self-occlusion never occurs even if I tilted the object at an infinitesimal angle. To satisfy the above assumptions, I consequently assume that there are no points where the zenith angle θ is equal to $90°$ except for the occluding boundary. By calculating the background subtraction image, the occluding boundary can be calculated; thus, the B-E region is easily determined.

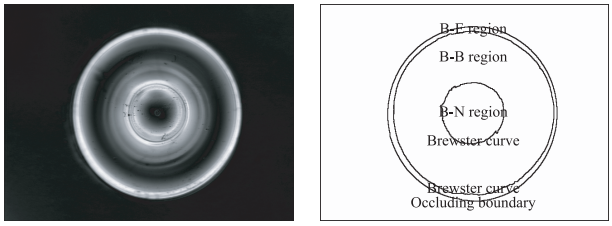

(a) (b)

Fig. 8: (a) A gray image of obtained degree of polarization of the bell-shaped object and (b) the result of Brewster segmentation.

4.2.2. B-N Region

The B-N region is the region which includes the point(s) mapped onto the North Pole on the Gaussian sphere. As shown in Figure 3, the region is mapped to a spherical cap on the Gaussian sphere, enclosed by a small circle mapped from the Brewster curve. The North Pole is located at the center of this spherical cap. The zenith angle of all the points in this region is in the range of $0° \leq \theta \leq \theta_B$. From the graph in Figure 3, I can also conclude that, in this range, the correspondence between θ and ρ is one-to-one, and I can also determine the zenith angle from the observed DOP.

If the DOP ρ equals to 0, the zenith angle θ will be $0°$ or $90°$. However, since I assume that the points where the zenith angle θ is equal to $90°$ only appear at the occluding boundary, the B-N region is determined only by searching the point where the degree of polarization equals to zero.

4.2.3. B-B Region

The B-B region is defined as the region which includes neither the occluding boundary nor the North Pole points and is bounded by one or more Brewster curves. The region which is neither the B-E region nor the B-N region is the B-B region. In the following sections, I will propose a method for disambiguating B-B regions.

4.3. Folding Curve

There are two possibilities for the existence of the B-B region on the Gaussian sphere. The B-B region is either on the northern side of the Brewster curve or on the southern side of the Brewster curve. The B-B region mapped onto the Gaussian sphere is bounded by one Brewster curve and one or more extra curves (Figure 6). By considering the points in the B-B region on Gaussian sphere, I find that there is one extreme point — northernmost or southernmost — in each azimuth angle. I denote the set of these points to be a folding curve. Now, I will prove that the folding curve is a geometrical invariant; Gaussian curvature at folding curve will be zero.

Theorem *Any folding curve on an object surface is a parabolic curve on that object surface. That is to say, at any surface point on a folding curve, the Gaussian curvature at the surface point vanishes.*

Proof. A surface normal can be represented in gradient space, a space constructed by gradients p and q:

$$p = \frac{\partial H}{\partial x}\,, \quad q = \frac{\partial H}{\partial y}\,, \tag{20}$$

where $H = H(x, y)$ denotes the height of the object surface. A folding curve is an extremum not only in a Gaussian sphere, but also in gradient space, $p = p(x, y)$ and $q = q(x, y)$. Therefore, one or both of the following equation holds:

$$\frac{\partial p}{\partial x} = \frac{\partial p}{\partial y} = 0 \tag{21}$$

$$\frac{\partial q}{\partial x} = \frac{\partial q}{\partial y} = 0\,. \tag{22}$$

Hessian $\mathcal{H}$ and Gaussian curvature K are related by the following equation:

$$\mathrm{sgn}K = \mathrm{sgn}\det\mathcal{H} \quad , \tag{23}$$

where Hessian is defined as:

$$\mathcal{H} = \begin{pmatrix} \dfrac{\partial^2 H}{\partial x^2} & \dfrac{\partial^2 H}{\partial x \partial y} \\ \dfrac{\partial^2 H}{\partial y \partial x} & \dfrac{\partial^2 H}{\partial y^2} \end{pmatrix}\,. \tag{24}$$

Since (21) or (22) holds, from (20)-(24), $K = 0$ is finally obtained. □

A parabolic curve is a curve where Gaussian curvature is zero and Gaussian curvature of object surface does not change through object rotation. Therefore, I can conclude that the folding curve is intrinsic to an object and invariant from the viewer direction.

4.4. Corresponding Points

I will solve the ambiguity in the B-B region by comparing the data of the DOP of the object placed unrotated and that of the object rotated at a small angle (Figure 9). I compare the DOP at two points where the invariant property on the surface matches, and disambiguate the ambiguity problem.

The Gaussian mapping of the B-B region of the object surface onto the Gaussian sphere is depicted in Figure 6. The B-B region includes neither the occluding boundary nor the north pole point, and is bounded only by the Brewster curve; thus, the folding curve always appears.

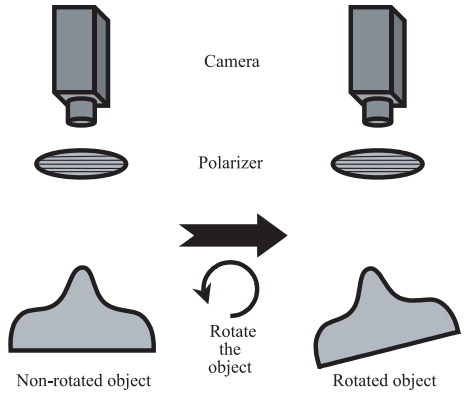

Fig. 9: Object rotation.

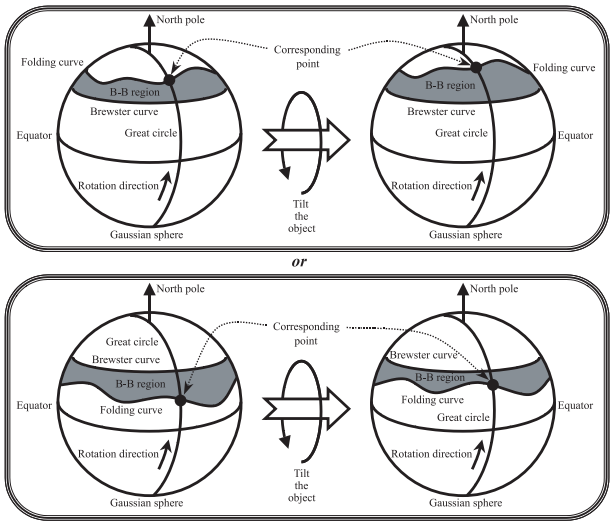

Fig. 10: Corresponding Point.

I define the corresponding point as the point where the folding curve and the great circle intersect (Figure 10). This great circle must be a cross-section between the Gaussian sphere and the plane which is parallel to the rotation direction of the object and includes the north pole of the Gaussian sphere. The surface point which is mapped onto this great circle, still maps onto this great circle after the object rotation, thus enabling unique matching.

To summarize:

1. If the B-B region is mapped onto the north of the Brewster curve, choose the northernmost point for the corresponding point which intersects the great circle; namely, choose the point where the DOP is minimum.
2. If the B-B region is mapped onto the south of the Brewster curve, choose the nearest point to the equa-

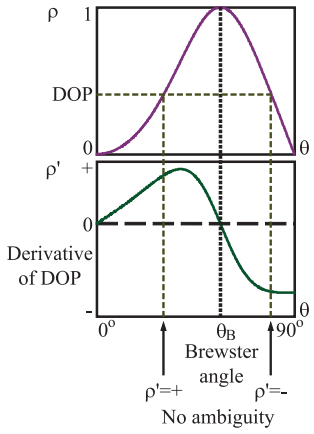

Fig. 11: Graph of derivative of DOP ($n = 1.5$).

tor for the corresponding point which intersects the great circle; namely, choose the point where the DOP is minimum.

4.5. Difference of Degree of Polarization

Finally, I describe the method used to resolve the ambiguity problem of the surface normal by comparing the DOP at the corresponding point of the nontilted object with that of the tilted object.

I regard the refractive index n as constant; thus, the DOP ρ is only a function of the zenith angle θ. The relationship between the rotation angle, $\Delta\theta$, the DOP of the nontilted object, $\rho(\theta)$, the DOP of the tilted object, $\rho(\theta + \Delta\theta)$, and the derivative of the DOP, $\rho'(\theta)$, will be:

$$\rho(\theta + \Delta\theta) - \rho(\theta) = \rho'(\theta)\Delta\theta \quad , \tag{25}$$

if $\Delta\theta$ is sufficiently small.

In fact, the absolute value of the rotation angle is not needed; however, I assume that the rotation direction is known. Since the azimuth angle ϕ has also already been determined, the sign of $\Delta\theta$ can be determined. As a result, by calculating the sign of the difference of two DOP values at the corresponding point and by giving the sign of $\Delta\theta$, I can determine, by using Equation (25), whether the zenith angle θ in B-B region is in the range of $0 \leq \theta \leq \theta_B$ or of $\theta_B \leq \theta \leq \pi/2$ (Figure 11).

5. Shape Estimation of Transparent Objects by using Polarization Raytracing

In this section, I introduce the method of estimating the shape by polarization raytracing.

5.1. Introduction

The two methods described in Section 3 and Section 4 focused on solving the ambiguity problem. However, these methods did not focus on solving the internal interrefleciton problem; they only considered the reflection and they did not consider the transmission. The method in this section focus on solving this internal interreflection problem by considering both reflection and transmission.

In this paper, a forward-facing surface of the transparent object is denoted as a frontal surface and an object surface facing away from the camera is denoted as a rear surface. The proposed method estimates the shape of the frontal surface by using polarization raytracing when the refractive index and the rear surface are given.

5.2. Inverse Polarization Raytracing

In this section, I introduce the proposed method for estimating the frontal surface shape of a transparent object using the DOP and the POI angle as inputs under the assumption that the refractive index and the backward-facing surface shape are given. Details of numerical algorithms and mathematics are shown in the literature [24, 25].

I denote the input polarization data as I_E. Polarization data are represented as an image(2-dimensionally distributed data) where the DOP and POI angle are set for each pixel. The polarizaiton raytracing explained in Section 2.2 can render the polarization data from the shape of transparent object. I denote such rendered polarization images as I_R. The shape of transparent objects is represented as the height H, set for each pixel. Heights partially differentiated by x and y are called gradient, and are represented as p and q, respectively:

$$p = H_x = \frac{\partial H}{\partial x}, \quad q = H_y = \frac{\partial H}{\partial y} \quad . \tag{26}$$

Surface normal $\mathbf{n} = (-p, -q, 1)^T$ is represented by these gradients. The rendered polarization image I_R depends upon height and surface normal, so it can be represented as $I_R(H, p, q)$. A straightforward definition of the cost function which I want to minimize can be as follows:

$$\iint E_1(x, y)dxdy \quad , \tag{27}$$

where,

$$E_1 = \left(I_E - I_R(H, p, q)\right)^2 \quad . \tag{28}$$

I will sometimes omit the variables (x, y) in the subsequent discussions for the simplicity of descriptions. I_R depends upon p, q, and H, while p, q, and H depend upon each other with Equation (26). Therefore, cost function must be modified as follows:

$$\iint (\lambda E_1 + E_2)\, dxdy \quad , \tag{29}$$

where,

$$E_2 = (H_x - p)^2 + (H_y - q)^2 \quad . \tag{30}$$

λ is Lagrange undetermined multiplier.

Euler equations which minimizes Equation (29) will be,

$$p = H_x - \frac{\lambda}{2}\frac{\partial E_1}{\partial p} \tag{31}$$

$$q = H_y - \frac{\lambda}{2}\frac{\partial E_1}{\partial q} \tag{32}$$

$$H = \bar{H} - \frac{1}{4}(p_x + q_y) - \frac{\lambda}{8}\frac{\partial E_1}{\partial H} \quad , \tag{33}$$

where $\bar{H}$ is a 4-neighbor average of H.

Each of the above Equations (31)(32)(33) can be decomposed into two steps:

$$p \leftarrow H_x \tag{34}$$

$$p \leftarrow p - \lambda_1 \frac{\partial E_1}{\partial p} \tag{35}$$

$$q \leftarrow H_y \tag{36}$$

$$q \leftarrow q - \lambda_2 \frac{\partial E_1}{\partial q} \tag{37}$$

$$H \leftarrow \bar{H} - \frac{1}{4}(p_x + q_y) \tag{38}$$

$$H \leftarrow H - \lambda_3 \frac{\partial E_1}{\partial H} \quad . \tag{39}$$

Here, λ_1, λ_2, and λ_3 are scalar values which are determined for each pixel and for each iteration step.

First, I set initial values of the shape H for each point of frontal surface. Next, p and q are calculated by Equations (34)(36). Then, I solve Equations (35)(37). λ_1 and λ_2 should be optimal values; thus, I use Brent's method to determine λ_1 and λ_2 which minimize the error function E_1. After computing p and q at every pixel, I solve Equation (38) by the relaxation method [26, 27] to determine the height H. I solved the relaxation problem by using the alternating-direction implicit method.

I do not choose to solve Equation (39) by Brent's method because the error function E_1 depends upon the change of surface normal rather than on the change of height. Another reason is that the error function E_1 smoothly changes when the surface normal changes, but it does not smoothly change when the height changes.

To conclude, the frontal surface shape of transparent object is estimated by an iterative computation, where each step of iteration solves Equations (34)–(38), and the iteration stops when Equation (27) is minimized.

6. Evaluations

In this section, I present some experimental results and evaluate the effectiveness of three proposed methods.

6.1. Experimental Setup

This section explains the experimental setup. Section 6.1.1 explains the experimental setup which obtains the polarization data of visible light. Section 6.1.2 explains the experimental setup which obtains the polarization data of infrared light.

6.1.1. Experimental Setup of Visible Light

Figure 12 represents our experimental setup, which I named "Cocoon", for obtaining the polarization data in visible light domain. The target object is set inside the center of the plastic sphere whose diameter is 35cm. This plastic sphere is illuminated by 36 incandescent lamps. These 36 light sources are almost uniformly distributed spatially around the plastic sphere by geodesic dome. The plastic sphere diffuses the light that comes from the light sources, and it behaves as a spherical light source, which illuminates the target object from every direction, which is located at the center of the sphere. This spherical diffuser provides an unpolarized light. The target object is observed by monochrome camera from the top of the plastic sphere, which has a hole on the top. Linear polarizer is set in front of the camera.

6.1.2. Experimental Setup of Infrared Light

Figure 13 shows the apparatus for the infrared light. Given that the infrared light is thermal radiation from a body and is not a reflection component, I do not use any light source. I increase the temperature of the object to 30-40 degrees Celsius by using a hair dryer to blow heated air over it. I also employ an infrared polarizer and an IR-CCD camera.

6.2. Experimental Results

This section explains the experimental result. Section 6.2.1 shows the measurement results of the first method,

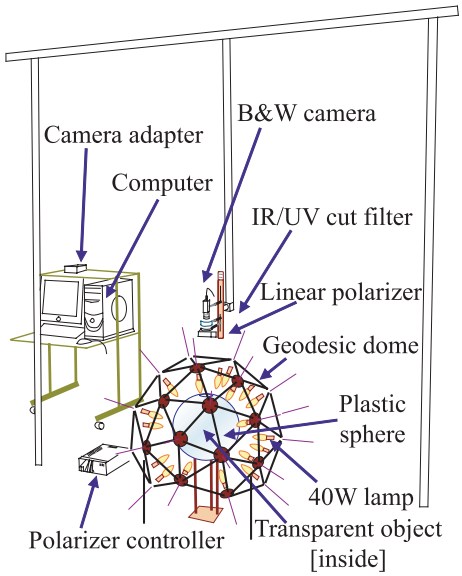

Fig. 12: Experimental setup for visible light.

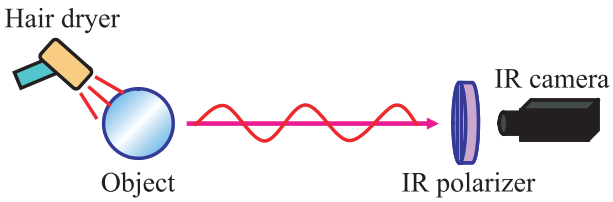

Fig. 13: Experimental setup for infrared light.

which uses thermal radiation. Section 6.2.2 shows the measurement results of the second method, which uses differential geometry. Section 6.2.3 shows the measurement results of the third method, which uses polarization raytracing.

6.2.1. Experimental Results of Thermal Radiation Method

This section shows the experimental results of the first method, which uses thermal radiation.

I determined the shape of the object shown in Figure 14(a). The shellfish-shaped object is made of acrylic and its refractive index is 1.5. The refractive index was obtained from the literature [28]. Figure 14(b) shows the obtained shape of the object.

6.2.2. Experimental Results of Differential Geometry Method

This section shows the experimental results of the second method, which uses differential geometry.

First, I used an acrylic transparent hemisphere whose

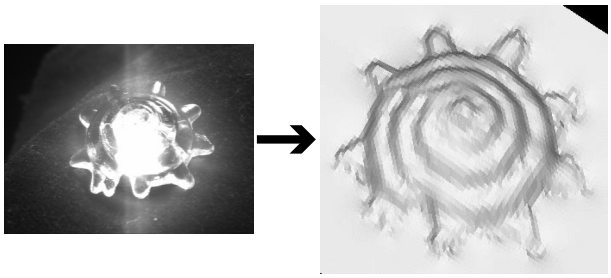

(a) Acrylic shellfish object (b) Obtained shape

Fig. 14: The resulting shape of the shellfish-shaped object

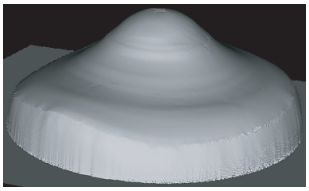

Fig. 15: A rendered image of the obtained shape of the bell-shaped object.

diameter was 30mm and refractive index was 1.5, obtained from the literature [28]. Error was calculated as an average value throughout the entire object surface, i.e., computed as an absolute difference between the true value and the obtained value. The errors of DOP, incident angle, and height were 0.17, 8.5°, and 1.1mm, respectively.

Next, I determined the shape of the bell-shaped object shown in Figure 7. The object was made of acrylic and its refractive index is 1.5, obtained from the literature [28]. The diameter(width) of the object was 24mm and the height was 8mm. I tilted the object approximately 8 degrees and obtained the data from two views. Figure 15 shows the rendered image of the estimated shape of the object. Figure 16 illustrates how the estimated shape fitted the true shape. Dots represent the obtained height and a solid line represents the true value, which was obtained by hand using the edge from the photo of the object observed from the side. An average error(=absolute difference) of the height was 0.4mm.

Another transparent object shown in Figure 17(a) was measured. This moutain-shaped object was made of epoxy and its refractive index was 1.6 [28]. The diameter(width) of the object was 45mm and the height was 25mm. Figure 17(b) shows the result of region segmentation. Here, one B-E region, one B-N region, and four

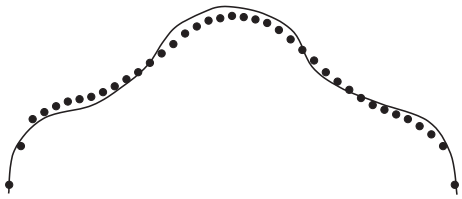

Fig. 16: The result of the real bell-shaped object.

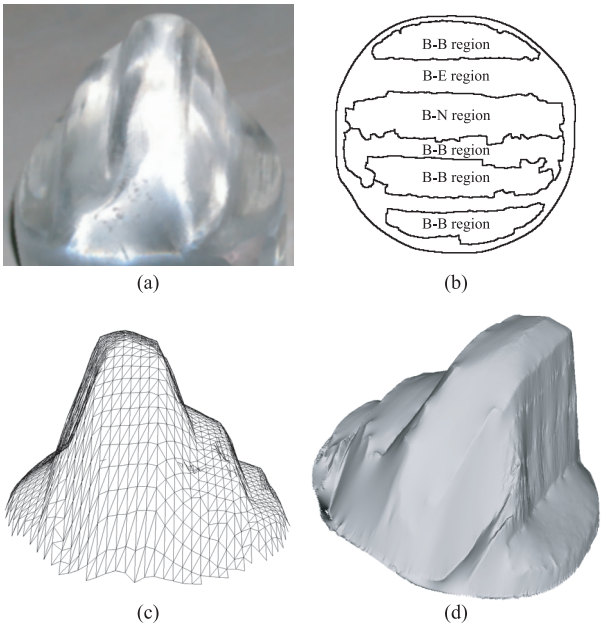

Fig. 17: Measurement result of transparent moutain-shaped object: (a) Real image, (b) region segmentation result, and (c) and (d) rendered image.

B-B regions are observed. I rotated the object approximately 8 degrees. Figure 17(c) and Figure 17(d) represent the estimated shape of the object.

6.2.3. Experimental Results of Inverse Polarization Raytracing Method

This section shows the experimental results of the third method, which uses polarization raytracing.

I observed an acrylic transparent hemisphere from the spherical part, whose refractive index was 1.5 and diameter was 30mm. The frontal surface was a hemisphere and rear surface was a disk. The camera was set orthogonal to the disk. I assumed that the illumination distribution is known.

The estimation result is shown in Figure 18. Figure 18(a) represents the result of Saito's method [9] and, at the same time, it represents the intial value. Figure 18(b)

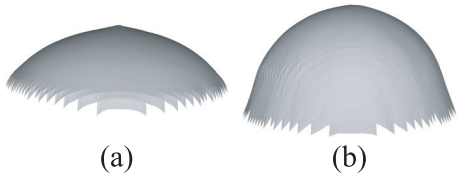

Fig. 18: 3D hemispherical object result: (a)Initial state, (b)result after 10 loop.

is the result after 10 loop of the method. The computation time was 36[sec] for 1 loop with 7,854 pixels by using Pentium4 3.4GHz. Here, the maximum number of the light ray traced is 10 reflection or transmission, however, if the energy of the light ray becomes less than a certain threshold, the tracing of the light ray is stopped.

In order to evaluate the estimation result in more detail, another evaluation was done in the 2D plane which was a cross section of the 3D object, which included the center of the base circle and the line perpendicular to that circle. A light ray which was inside this plane did not go out, and a light ray which was outside this plane did not come in. The proposed algorithm estimated the frontal surface shape, a semicircle, by using the polarization data of the 2D plane as input data.

The result of applying the proposed method is given in Figure 19(d). For comparison, the result of Saito's method [9] is shown in Figure 19(a). In Figure 19, the solid line represents the estimated shape, and the dotted line represents the true value. The shape computed by Saito's method(Figure 19(a)) is used as an initial value for Figure 19(d). Figure 19(b)(c)(d) is the result after 5, 25, and 50 loops, respectively.

The error value, Equation (27), is plotted in Figure 20. In Figure 20, vertical axis represents the value of Equation (27), and horizontal axis represents the number of iteration. The leftmost value is the error of Saito's method [9].

The computation time was 5.9[sec] for 1 loop with 320 pixels by using Pentium4 3.4GHz. Here, the maximum number of the light ray traced is 100 reflection or transmission, however, if the energy of the light ray becomes less than a certain threshold, the tracing of the light ray is stopped.

The RMS error between the estimated value and the true value was used to compare the accuracy between the proposed method and Saito's method. The RMS error of the

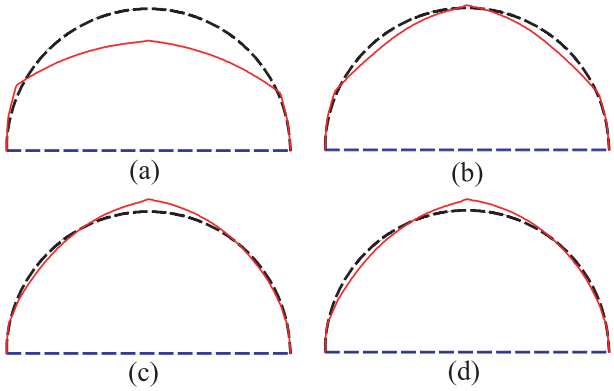

Fig. 19: Estimation result: (a) Result of Saito's method, (b)(c)(d) result after 5, 25, and 50 loops with proposed method, respectively.

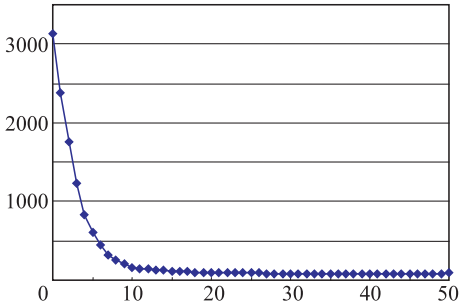

Fig. 20: Error for each loop.

surface normal was $13.5°$ for Saito's method and $7.02°$ for the proposed method. The RMS error of the height was 2.77mm for Saito's method and 0.607mm for the proposed method.

Next, I apply the method to the bell-shaped transparent object shown in Figure 7. The object is observed from the sticked-out part of the object. The frontal surface was the curved surface and rear surface was a disk. The camera was set orthogonal to the disk. I assumed that the illumination distribution is known. I estimated the shape of the cross-section of the object to analyze the precision of the proposed method. Figure 21(d) illustrates the estimated shape of the object. Solid curve represents the obtained frontal height, and dotted line represents the given rear height. Initial value is set to be a semicircle shown in Figure 21(a). Estimated shape after 1, 5, and 20 loops is illustrated in Figure 21(b), (c), and (d), respectively. True shape is represented as a solid curve in Figure 16. An error(=mean deviation) of the height was 0.24mm. The computation time was 7.0[sec] for 1 loop with 320 pixels

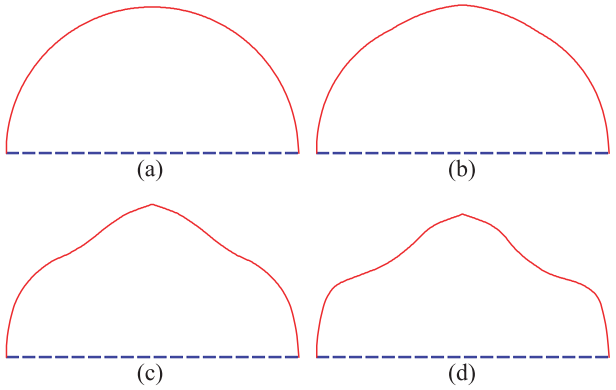

Fig. 21: Estimated shape of bell-shaped acrylic object by using the inverse polarization raytracing method: (a) initial value, (b)(c)(d) estimated after 1, 5, and 20 loops, respectively.

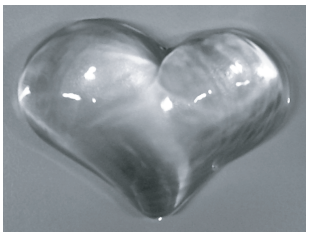

Fig. 22: A photograph of the heart-shaped object.

by using Pentium4 3.4GHz.

I also apply the method to the heart-shaped transparent object shown in Figure 22. The object was made of glass and its refractive index is 1.5, obtained from the literature [28]. The object is observed from the curved surface of the object. The frontal surface was the curved surface and rear surface was a planar surface. The camera was set orthogonal to the rear surface. I assumed that the illumination distribution is known. The estimation result is shown in Figure 23. Figure 23(a) represents the result of Saito's method [9] and, at the same time, it represents the intial value. Figure 23(b) is the result after 10 loop of the method. Figure 23(c) is rendered example of raytracing method by using the estimated shape.

7. Conclusion

7.1. Summary

In this paper, I have proposed three methods for determining the shape of a transparent object by using polarization filter. Algorithm that uses only one view in visible light domain results in ambiguities. The first method

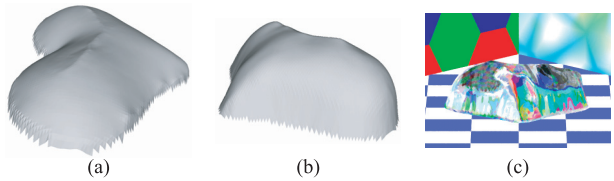

(a) (b) (c)

Fig. 23: Result of heart-shaped object: (a)Initial state, (b)result after 10 loop, (c)raytraced image.

solves this ambiguity problem by employing the polarization in infrared light domain, and the second method solves it by employing the polarization of a slightly tilted view. These two methods still have a problem that they do not consider the internal interreflection. The third method solves this internal interrefleciton problem by employing the polarization raytracing algorithm. The ambiguty problem and the polarization raytracing algorithm are presented in Section 2.

First method [29] The thermal radiation, which also has characteristics of polarization, can be observed as infrared light. This polarization is an one-valued function; measuring degree of polarization in infrared domain provides the unique zenith angle. However, the degree of polarization is relatively low, and in some cases it is difficult to determine the degree of polarization precisely. Therefore, I propose to use polarization in both visible and infrared light. This method is presented in Section 3.

Second method [30] By rotating the object, the ambiguity problem can be also solved. Two sets of data are obtained: One is from the object not tilted, and the other is from the object tilted at a small angle. These data are segmented into some regions with regard to the Brewster angle. Then, the method calculates the difference of the degree of polarization between these two sets of data at the corresponding point — the point where surface normal lies along the rotation direction and where the degree of polarization is minimum in the B-B region. From that difference, the correct surface normal is determined. This method is presented in Section 4.

Third method [31] Solving the inverse problem of polarization raytracing method, the shape of transparent objects can be estimated more precisely. Polarization raytracing method considers the internal interreflection. To obtain the shape of transparent object, the method minimizes the difference between the input polarization data taken by observing the transparent object and the computed polarization data rendered by the polarization raytracing method. This method is presented in Section 5.

I have implemented these proposed methods, and demonstrated their abilities to determine the shape of transparent objects. Experiments are presented in Section 6.

7.2. Future Work

The future work is to obtain the shape of transparent objects more accurately. I also intend to develop a method which can measure the refractive index at the same time as well as the surface shape of transparent object. By collaborating with a company, I am trying to develop a polarization camera [32], which measures the polarization state of the light more faster than existing realtime polarization camera [33–35]. Another future work is to develop a commercial product for measuring the shape of transparent object by collaborating with a camera manufacturer. I am also planning to collaborate with scientists of physics to obtain some advices to make my methods more robustly by using the professional knowledges in the field of physics.

There are many beautiful glass objects of art in all over the world. The proposed method will be useful for modeling such glass objects of art. Other application field of the modeling of transparent objects can range from computer-aided manufacturing, classifying garbage/rubbish for recycling glass and plastic bottles, to creating 3D catalogs for online shopping, etc. For the first step for such a wide area of applications, I proposed a basic technique for modeling the surface shape of transparent objects.

Acknowledgments

Daisuke Miyazaki was supported by the Research Fellowships of the Japan Society for the Promotion of Science for Young Scientists.

References

[1] K. Koshikawa and Y. Shirai, “A model-based recognition of glossy objects using their polarimetrical properties,” *Advanced Robotics*, vol. 2, no. 2, pp. 137–147, 1987.

[2] L. B. Wolff and T. E. Boult, “Constraining object features using a polarization reflectance model,” *IEEE Trans. Pat-*

tern Analysis and Machine Intelligence, vol. 13, no. 7, pp. 635–657, 1991.

[3] S. Rahmann, "Inferring 3D Scene Structure from a Single Polarization Image," in *SPIE Proc. Conf. Polarization and Color Techniques in Industrial Inspection*, vol. 3826, pp. 22–33, Munich, Germany, 1999.

[4] S. Rahmann, "Polarization images: a geometric interpretation of shape analysis," in *Proc. Int'l Conf. Pattern Recognition*, pp. 542–546, Barcelona, Spain, 2000.

[5] S. Rahmann and N. Canterakis, "Reconstruction of specular surfaces using polarization imaging," in *Proc. Int'l Conf. Computer Vision and Pattern Recognition*, pp. 149–155, Kauai Marriott, Hawaii USA, 2001.

[6] S. Rahmann, "Reconstruction of quadrics from two polarization views," in *Proc. Iberian Conf. Pattern Recognition and Image Analysis*, pp. 810–820, Mallorca, Spain, 2003.

[7] O. Drbohlav and R. Šára, "Unambiguous determination of shape from photometric stereo with unknown light sources," in *Proc. IEEE Int'l Conf. Computer Vision*, pp. I:581–586, Vancouver, Canada, 2001.

[8] D. Miyazaki, R. T. Tan, K. Hara, and K. Ikeuchi, "Polarization-based inverse rendering from a single view," in *Proc. IEEE Int'l Conf. Computer Vision*, pp. 982–987, Nice, France, 2003.

[9] M. Saito, Y. Sato, K. Ikeuchi, and H. Kashiwagi, "Measurement of surface orientations of transparent objects by use of polarization in highlight," *J. Optical Society of America, A*, vol. 16, no. 9, pp. 2286–2293, 1999.

[10] H. Murase, "Surface shape reconstruction of a nonrigid transparent object using refraction and motion," *IEEE Trans. Pattern Analysis and Machine Intelligence*, vol. 14, no. 10, pp. 1045–1052, 1992.

[11] S. Hata, Y. Saitoh, S. Kumamura, and K. Kaida, "Shape extraction of transparent object using genetic algorithm," in *Proc. Int'l Conf. Pattern Recognition*, pp. 684–688, Vienna, Austria, 1996.

[12] K. Ohara, M. Mizukawa, K. Ohba, and K. Taki, "3D modeling of micro transparent object with integrated vision," in *Proc. IEEE Conf. Multisensor Fusion and Integration for Intelligent Systems*, pp. 107–112, Tokyo, Japan, 2003.

[13] M. Ben-Ezra and S. K. Nayar, "What does motion reveal about transparency?," in *Proc. IEEE Int'l Conf. Computer Vision*, pp. 1025–1032, Nice, France, 2003.

[14] M. Born and E. Wolf, *Principles of optics*, Pergamon Press, London, 1959.

[15] W. A. Shurcliff, *Polarized light: production and use*, Harvard University Press, Cambridge, Mass., 1962.

[16] O. Sandus, "A review of emission polarization," *Applied Optics*, vol. 4, no. 12, pp. 1634–1642, 1965.

[17] F. E. Nicodemus, "Directional reflectance and emissivity of an opaque surface," *Applied Optics*, vol. 4, pp. 767–773, 1965.

[18] F. E. Nicodemus, "Reflectance nomenclature and directional reflectance and emissivity," *Applied Optics*, vol. 9, pp. 1474–1475, 1970.

[19] D. L. Jordan and G. D. Lewis, "Measurements of the effect of surface roughness on the polarization state of thermally emitted radiation," *Optical Letters*, vol. 19, pp. 692–694, 1994.

[20] D. L. Jordan, G. D. Lewis, and E. Jakeman, "Emission polarization of roughened glass and aluminum surfaces," *Applied Optics*, vol. 35, pp. 3583–3590, 1996.

[21] L. B. Wolff, A. Lundberg, and R. Tang, "Image understanding from thermal emission polarization," in *Proc. IEEE Conf. Computer Vision and Pattern Recognition*, pp. 625–631, Santa Barbara, CA USA, 1998.

[22] M. P. do Carmo, *Differential geometry of curves and surfaces*, Prentice-Hall, New Jersey, 1976.

[23] B. K. P. Horn, *Robot vision*, MIT Press, Cambridge, Mass., 1986.

[24] W. H. Press, S. A. Teukolsky, W. T. Vetterling, and B. P. Flannery, *Numerical recipes in C: the art of scientific computing*, Cambridge University Press, Cambridge, England, 1992.

[25] R. Courant and D. Hilbert, *Methods of mathematical physics*, Wiley, New York, 1953.

[26] K. Ikeuchi, "Reconstructing a depth map from intensity maps," in *Proc. Int'l Conf. Pattern Recognition*, pp. 736–738, Montreal, Canada, 1984.

[27] B. K. P. Horn, "Height and Gradient from Shading," *Int'l J. Computer Vision*, vol. 5, no. 1, pp. 37–75, 1990.

[28] J. F. Shackelford, W. Alexander, and J. S. Park, *CRC Materials Science and Engineering Handbook*, CRC Press, Boca Raton, Fla., 1994.

[29] D. Miyazaki, M. Saito, Y. Sato, and K. Ikeuchi, "Determining surface orientations of transparent objects based on polarization degrees in visible and infrared wavelengths," *J. Optical Society of America, A*, vol. 19, no. 4, pp. 687–694, 2002.

[30] D. Miyazaki, M. Kagesawa, and K. Ikeuchi, "Transparent surface modeling from a pair of polarization images," *IEEE Trans. Pattern Analysis and Machine Intelligence*, vol. 26, no. 1, pp. 73–82, 2004.

[31] D. Miyazaki and K. Ikeuchi, "Inverse Polarization Raytracing: Estimating Surface Shape of Transparent Objects," in *Proc. Int'l Conf. Computer Vision and Pattern Recognition*, San Diego, CA USA, 2005 to appear.

[32] Furuuchi Chemical Corporation, `http://www.furuchi.co.jp/`.

[33] L. B. Wolff, T. A. Mancini, P. Pouliquen, and A. G. Andreou, "Liquid Crystal Polarization Camera," *IEEE Tran. Robotics and Automations*, vol. 13, no. 2, pp. 195–203, 1997.

[34] H. Fujikake, K. Takizawa, T. Aida, H. Kikuchi, T. Fujii, and M. Kawakita, "Electrically-Controllable Liquid Crystal Polarizing Filter for Eliminating Reflected Light," *Optical Review*, vol. 5, no. 2, pp. 93–98, 1998.

[35] C. K. Harnett and H. G. Craighead, "Liquid-crystal micropolarizer array for polarization-difference imaging," *Applied Optics*, vol. 41, no. 7, pp. 1291–1296, 2002.